Supplementary material: Raman imaging of twist angle variations in twisted bilayer graphene at intermediate angles

A. Schäpers,[1,*] J. Sonntag,[1,2,*] L. Valerius,[1] B. Pestka,[3] J. Strasdas,[3] K. Watanabe,[4] T. Taniguchi,[5] L. Wirtz,[6] M. Morgenstern,[3] B. Beschoten,[1,†] R. J. Dolleman,[1] and C. Stampfer[1,2]

[1] *JARA-FIT and 2nd Institute of Physics, RWTH Aachen University, 52074 Aachen, Germany*
[2] *Peter Grünberg Institute (PGI-9), Forschungszentrum Jülich, 52425 Jülich, Germany*
[3] *2nd Institute of Physics B and JARA-FIT, RWTH Aachen University, 52074 Aachen, Germany*
[4] *Research Center for Functional Materials, National Institute for Materials Science, 1-1 Namiki, Tsukuba 305-0044, Japan*
[5] *International Center for Materials Nanoarchitectonics, National Institute for Materials Science, 1-1 Namiki, Tsukuba 305-0044, Japan*
[6] *Department of Physics and Materials Science, University of Luxembourg, 162a avenue de la Faïencerie, L-1511 Luxembourg, Luxembourg*

I. DETAILS ON THE SAMPLE FABRICATION

The fabrication technique to produce flipped half-stacks of tBLG is based on the tear and stack method, thus ensuring control over the twist angle between the graphene lattices [1, 2]. To flip the samples, the method is adapted by exploiting the water solubility of polyvinyl alcohol (PVA) [3]. In the first step of fabrication, a piece of polydimethylsiloxane (PDMS, Gelpack) approximately 5 by 5 mm is placed on a 20 by 20 mm microscope cover glass (Fig. S1a). A small droplet of a 5 % solution of PVA (Sigma Aldrich, M_w 9,000-10,000, 80% hydrolyzed) in water is dropped on the PDMS square (Fig. S1b), leaving behind a thin layer of PVA after the water has evaporated (Fig. S1c). For the further process, it is important that the PVA does not reach over the edge of the PDMS. We use mechanically exfoliated hBN and graphene flakes on 90 nm of SiO_2/Si^{++} dies, which are placed on a heated stage that is able to rotate (Fig. S2a). The PMDS/PVA stamp is placed upside-down in a setup with a micromanipulator, to pick up the flakes from substrate as shown in Fig. S2. The hBN flake is picked up first, followed by the tear-and-stack procedure to pick up the graphene flakes with the desired twist angle, as illustrated in Fig. S3.

When the stack is assembled, the order of materials is as follows: tBLG - hBN - PVA- PDMS - glass slide. Now, a second polymer stamp is prepared on a glass slide, consisting of a square of PDMS with a long and rectangular strip of thin poly(bisphenol A carbonate) (PC) laying across it. The two outer ends of the PC strip are hanging over the edge of the PDMS square and they are taped to the glass slide. Also, the area of PDMS covered by the PC strip has to be larger than the patch of PVA. In the next step, the layer of PVA with the sample on it is transferred from the first polymer stamp to the second stamp with PC. Using the transfer system, the PVA stamp is placed on top of the PC stamp at 80 °C (Figs. S4a-b). It is important to place the patch of PVA exactly on that area of PC which covers the PDMS. The high temperature ensures that when removing the upper stamp, the PVA will detach from the PDMS (Fig. S4c), leaving the following order of materials from up to down on the PC stamp: PVA - hBN - tBLG - PC - PDMS - glass slide. To remove the PVA from the top of the stamp, the entire glass slide is put into water for at least ten minutes (Fig. S4d). After this, the hBN - tBLG sample is again located at the surface of the stamp. Finally, the tapes fixing the outer edges of the PC strip to the glass are removed. Alternatively, the PC strip can be cut in a way that leaves the central piece of PC covering the PDMS free to be transferred, without damaging the sample. At a

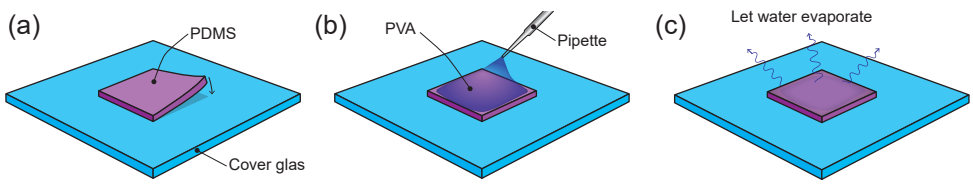

FIG. S1. Preparation of the polymer stamp. (a) A PDMS stamp is placed on the microscope cover glass. (b) A droplet of PVA solution is placed on the stamp. (c) After the water has evaporated, the stamp is ready for use.

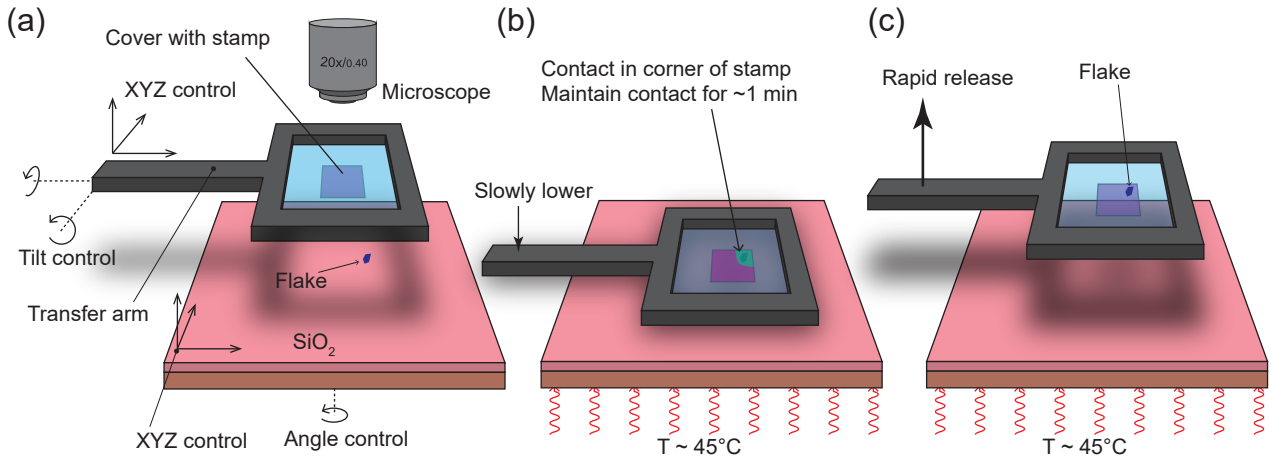

FIG. S2. Pick-up of exfoliated flakes. (a) The stamp is placed upside-down on a arm connected to a micromanipulator, and held in place by a vacuum. (b) The stamp is slowly brought into contact with the flake while the substrate is heated to 45°. (c) After one minute, the flake is picked up by rapidly moving the arm upward.

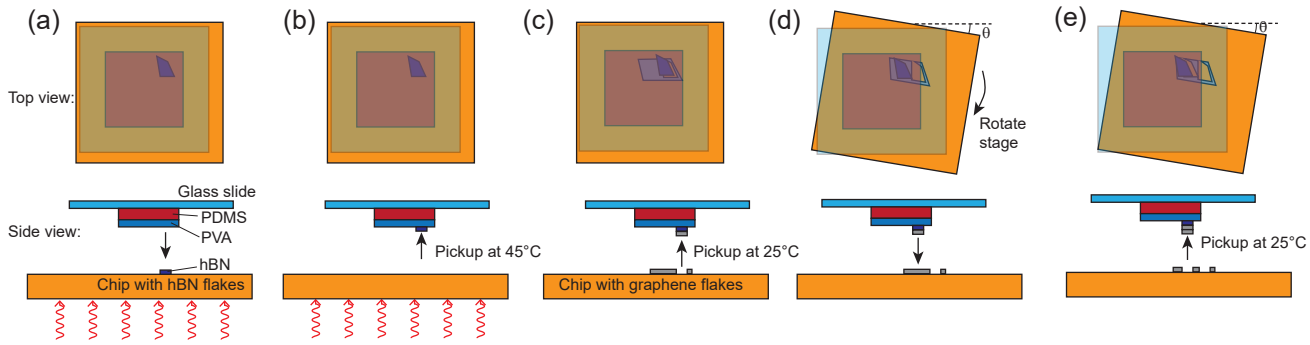

FIG. S3. Tear and stack method to assemble the twisted bilayer graphene heterostructure on the stamp.

temperature of roughly 100 °C, the hBN - tBLG - PC part of the stamp is transferred onto a SiO_2/Si^{++} chip (Figs. S4e-g). After removing the PC with chloroform (Fig. S4h), the flipped half-sandwich of tBLG on hBN is ready.

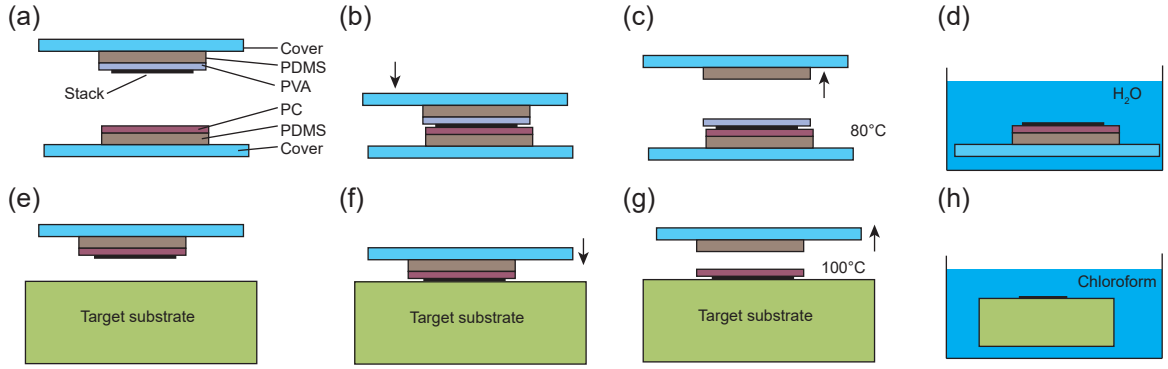

FIG. S4. Flipping the assembled stack and transferring to the final target substrate.

II. DETAILS ON RAMAN SPECTROSCOPY MEASUREMENTS

The Raman measurements are performed in a commercial micro-Raman setup manufactured by WITec GmbH with an excitation wavelength of $\lambda = 532\,\mathrm{nm}$. The laser power typically used is $5\,\mathrm{mW}$. The laser is focused onto a sample via a $100\times$ (NA $= 0.9$) objective to a spot with a FWHM of $\sim 520\,\mathrm{nm}$, see Figure S5. For the detection of the

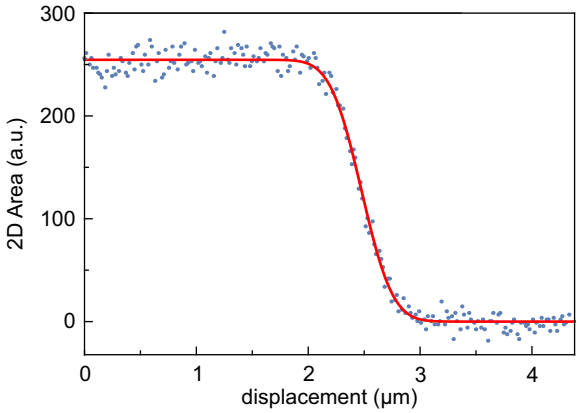

FIG. S5. Intensity of the 2D Raman peak along along a path perpendicular to the edge of a graphene flake. As the edge of the flake is atomically sharp, the intensity profile is a convolution of a step function with a Gaussian function. We thus determine the laser spot size by fitting the intensity with an error function $I(x) = I_0\mathrm{erf}(\frac{(x-x_0)}{r})$, in which r is the radius of the Gaussian profile and x_0 is the position of the edge. The result of the fit results in a laser spot FWHM of $(518 \pm 14)\,\mathrm{nm}$.

scattered light, we employ a CCD spectrometer with a grating of 1200 lines/mm when investigating ω_{TA} or the G and 2D peak. To extract a meaningful value of the width of the TA peak Γ_{TA} we employ a higher resolution grating of 2400 lines/mm. The higher resolution grating is used for the analysis of the width of the TA peak Γ_{TA}, i.e., in the measurements shown in the zoom-in of Figure 2e and Figure 3 in the main text. The typical integration time for mapping is $5\,\mathrm{s}$.

3. SCANNING TUNNELING MICROSCOPY

The flipped stacks of Si/SiO_2/hBN/tBLG are contacted by a shadow mask evaporation of Au at $300\,\mathrm{K}$. Afterwards the sample is transferred into a home-built ultrahigh vacuum scanning tunneling microscope (STM) operating at $300\,\mathrm{K}$ [4] without further treatment. The instrument is equipped with a long-distance microscope to find flakes within the STM. W-tips, that are prepared on Au(111) priorily, are employed for STM images of the tBLG at sample voltage $V = 300\,\mathrm{mV}$ and current $I = 0.9\,\mathrm{nA}$. The twist angle has been determined from the moiré periodicity using the simultaneously measured atomic periodicity as calibration.

Comparison to Raman experiment

Figure S6a shows a zoom-in of the Raman map shown in Figure 2e of the main text. It is difficult to accurately know the position where the STM map is recorded. Therefore, we marked the area after the measurement by piercing it with the STM tip, resulting in optically visible damage to the sample. The position and shape of the damaged area is marked by the ellipse in Figure S6a. Within this region, ω_{TA} varies between 253 cm^{-1} and 271 cm^{-1}. Using our model as described in the main text, this results in twist angles between 6.76° and 7.24°.

The STM map is shown in Figure S6b. From the Fourier transformation (inset), we estimate the moiré wavelength to be $(1.91 \pm 0.10)\,\mathrm{nm}$, resulting in a twist angle of $(7.39 \pm 0.40)°$ [5]. This confirms that the twist angle θ_{TA} determined by Raman spectroscopy is close to the actual twist angle θ present in the sample.

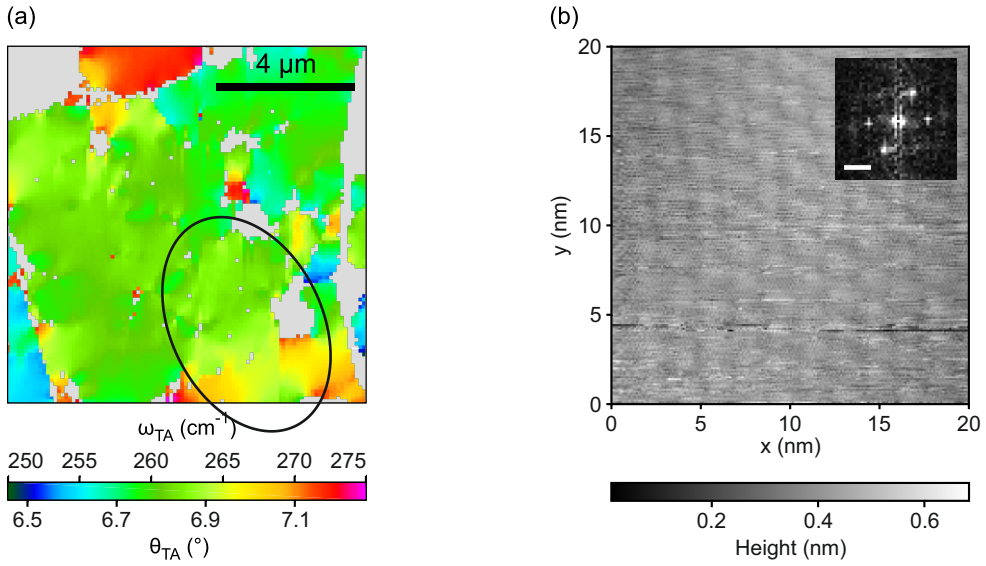

FIG. S6. Comparison between Raman and STM measurements. (a) Zoom-in of the Raman map in Fig. 2e. The black ellipse indicates the approximate area where the STM measurement is taken. (b) STM map taken within the indicated region. The moiré wavelength is (1.91 ± 0.10) nm, corresponding to a twist angle of $(7.39 \pm 0.40)°$. The inset shows a Fourier transformation of the STM map with a scale bar of $0.5\,\mathrm{nm}^{-1}$.

4. DISCUSSION ON INACCURACY IN THE TWIST ANGLE ESTIMATION

Here, we discuss the accuracy of our method to determine the absolute twist angle. The association of the frequency of the activated TA mode with a particular twist angle θ hinges on several assumptions or approximations of the phonon dispersion. We identified several effects that may lead to an inaccuracy of the twist angle estimation that we address below.

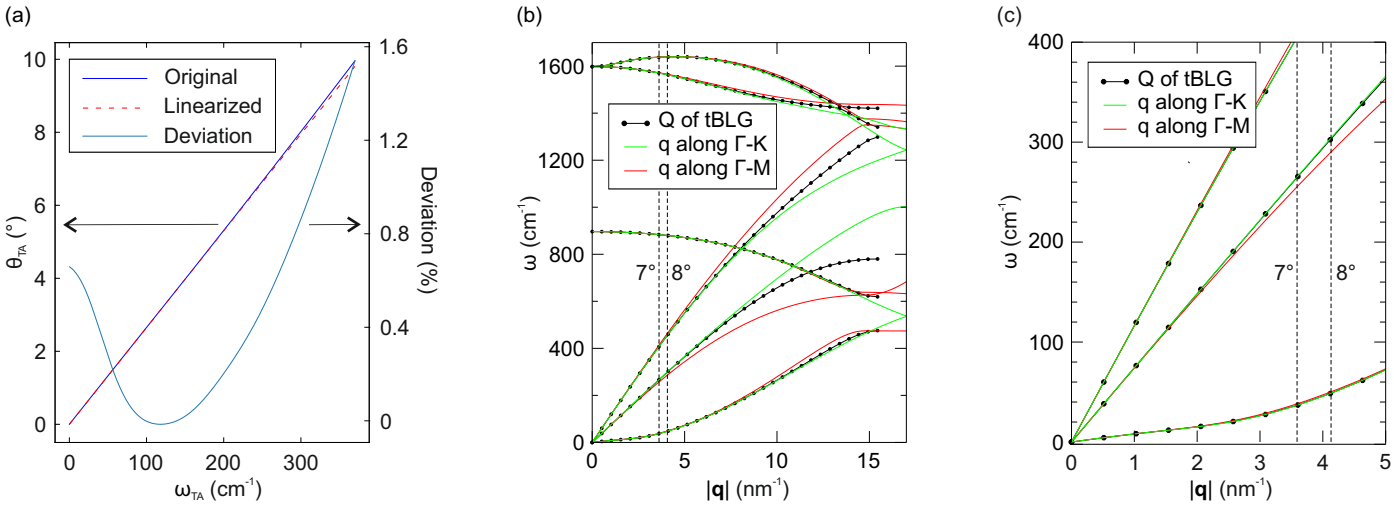

FIG. S7. Details on the sources of systematic inaccuracy in twist angle calculation. (a) The effect of linearizing the TA phonon branch is illustrated by comparing the transformation of TA peak position ω_{TA} into twist angle θ_{TA} using the original dispersion (dark blue line) and the linearized dispersion (dashed red line). The light blue line shows the deviation between the two methods. (b) SLG band structure calculation along high-symmetry axes Γ-M, Γ-K and along the lattice vector of the mini-Brillouin zone. (c) Zoom-in into the calculation shown in panel (b) showing the range of crystal momentum $|\mathbf{q}|$ corresponding to twist angles from 0° to $\sim 10°$.

Effect of the band dispersion linearization

In the frequency range relevant for the analysis of low and intermediate twist angles, the TA phonon branch of graphene is almost linear. As described in the main text, the phonon branch is linearized for the sake of simplicity in calculation. In Figure S7a, we show how the linearization of the phonon dispersion affects the transformation of TA peak position ω_{TA} into twist angle θ_{TA} by comparing it to a transformation that was done using the original phonon dispersion. The maximal deviation is $\sim 1.5\,\%$ for twist angles $\theta < 10^\circ$, as stated in the main text.

Effect of the phonon dispersion calculation

The translation of the TA peak position into the twist angle depends sensitively on the TA phonon dispersion. The calculation of the phonon dispersion was performed as in Ref. [6], using density functional theory in the local-density approximation (LDA) for the exchange-correlation functional. Using the generalized-gradient approximation (GGA) yields almost exactly the same TA phonon dispersion (albeit the GGA lattice constant is 0.3% larger than the LDA one). The TA mode at K is at 1001.3 cm^{-1} in LDA and at 1001.8 cm^{-1} in GGA[6] which means that the slope of the TA mode differs by less than 0.1% between the two approximations.

One may wonder about the effect of layer-layer interaction on the slope of the TA mode. Here, we use the difference in the TA mode frequency at K between graphene (1001.3 cm^{-1}) and graphite (1001.9 cm^{-1}) which again gives a negligible impact on the slope of the TA branch (compared to the other sources of uncertainty discussed below).

Effect of substrate and strain

We expect a larger influence to come from the graphene substrate interaction via doping and/or strain effects. To estimate the impact of this effect, we consider the sound velocity of the TA phonon branch, v_{TA}, in the Γ-M direction. From our phonon dispersion, we find $v_{\mathrm{TA}}^{\mathrm{theo}} = 13.8\,\mathrm{km/s}$. while a recent experimental study of graphene on SiO_2, using resonant Raman spectroscopy, determined a value of $v_{\mathrm{TA}}^{\mathrm{exp}} = 12.9\,\mathrm{km/s}$ [7]. The difference in slope by about 9% may be taken as a measure for the error bar that gives an indication by about how much the real TA mode slope deviates from the ab-initio value.

A similar error bar for experimental TA slopes can be obtained by looking at the comparison of electron energy loss spectroscopy (EELS) dispersions [8–10] of graphene on different substrates with ab-initio calculations [6].

Effect of the moiré lattice vector direction

Another simplification consists in using the phonon dispersion along the high-symmetry axis Γ-K to transform the position of the TA peak into the length

$$Q(\theta) = |\mathbf{b}^{\mathrm{s}}_{1,2}(\theta)| = \frac{8\pi}{\sqrt{3}a}\sin\left(\frac{\theta}{2}\right) \tag{S1}$$

of the lattice vector of the mini-Brillouin zone (eq. 1 in the main text). This would be true only if $\mathbf{b}^{\mathrm{s}}_{1,2}(\theta)$ always pointed along the Γ-K axis. This is approximately true for very small twist angles, but, in principle, both the length and the direction of these vectors depend on the twist angle. In terms of reciprocal unit vectors $\hat{\mathbf{k}}_x$ and $\hat{\mathbf{k}}_y$, they can be expressed as [5]

$$\mathbf{b}^{\mathrm{s}}_{1,2}(\theta) = \frac{2\pi}{\sqrt{3}a}\left[[\mp(1-\cos(\theta)) - \sqrt{3}\sin(\theta)]\hat{\mathbf{k}}_x + [-\sqrt{3}(1-\cos(\theta)) \pm \sin(\theta)]\hat{\mathbf{k}}_y\right]. \tag{S2}$$

To confirm that the simplification to follow the Γ-K direction is valid nonetheless, we present in Figs. S7b-c a calculation of the phonon dispersion along the path defined in reciprocal space by eq. S2 for twist angles from 0° to 30°. For small twist angles, this path starts along the Γ-K direction, but then bends away from it and ends, for θ =30°, half way between K and M on the edge of the first Brillouin zone. We compare the phonon dispersion along this line to the phonon dispersion calculated along the high-symmetry axes Γ-K and Γ-M. The dashed vertical lines denote twist angles of 7° and 8°. In the regime of the twist angles that are relevant for this work, the dispersion along the path defined by eq. S2 lies very close to the dispersion in Γ-K direction. Namely, for the TA mode at the wave vector corresponding to 8°, the deviation in frequency is $0.85\,\mathrm{cm}^{-1}$, which corresponds to a deviation in twist angle of 0.02°.

Inaccuracy in twist angle determination

Based on the analysis of the different sources of uncertainty above, we find that in our twist angle range the uncertainty from the effect of substrate and strain significantly larger than the others. We thus take the 9% uncertainty found here as the uncertainty in the dispersion that we use to determine our inaccuracy and precision in the main text. As stated in the main text, this uncertainty in the slope tranlates into an uncertainty of the *absolute* value of the twist angle, but only marginally affects the experimental determination of twist angle *variations*.

---

* These authors contributed equally.
† Corresponding author: bernd.beschoten@physik.rwth-aachen.de

[1] K. Kim, M. Yankowitz, B. Fallahazad, S. Kang, H. C. P. Movva, S. Huang, S. Larentis, C. M. Corbet, T. Taniguchi, K. Watanabe, S. K. Banerjee, B. J. LeRoy, and E. Tutuc, "van der Waals Heterostructures with High Accuracy Rotational Alignment," Nano Lett. **16**, 1989–1995 (2016).
[2] Y. Cao, J. Y. Luo, V. Fatemi, S. Fang, J. D. Sanchez-Yamagishi, K. Watanabe, T. Taniguchi, E. Kaxiras, and P. Jarillo-Herrero, "Superlattice-Induced Insulating States and Valley-Protected Orbits in Twisted Bilayer Graphene," Phys. Rev. Lett. **117**, 116804 (2016).
[3] D. Wong, K. P. Nuckolls, M. Oh, B. Lian, Y. Xie, S. Jeon, K. Watanabe, T. Taniguchi, B. A. Bernevig, and A. Yazdani, "Cascade of electronic transitions in magic-angle twisted bilayer graphene," Nature **582**, 198–202 (2020).
[4] V. Geringer, M. Liebmann, T. Echtermeyer, S. Runte, M. Schmidt, R. Rückamp, M. C. Lemme, and M. Morgenstern, "Intrinsic and extrinsic corrugation of monolayer graphene deposited on SiO_2," Phys. Rev. Lett. **102**, 076102 (2009).
[5] V. Carozo, C. M. Almeida, E. H. M. Ferreira, L. G. Cançado, C. A. Achete, and A. Jorio, "Raman signature of graphene superlattices," Nano Lett. **11**, 4527–4534 (2011).
[6] L. Wirtz and A. Rubio, "The phonon dispersion of graphite revisited," Solid State Commun. **131**, 141–152 (2004).
[7] X. Cong, Q.-q. Li, X. Zhang, M.-l. Lin, J.-b. Wu, X.-l. Liu, P. Venezuela, and P.-h. Tan, "Probing the acoustic phonon dispersion and sound velocity of graphene by Raman spectroscopy," Carbon **149**, 19–24 (2019).
[8] C. Oshima, T. Aizawa, R. Souda, Y. Ishizawa, and Y. Sumiyoshi, "Surface phonon dispersion curves of graphite (0001) over the entire energy region," Solid State Commun. **65**, 1601–1604 (1988).
[9] S. Siebentritt, R. Pues, K.-H. Rieder, and A. M. Shikin, "Surface phonon dispersion in graphite and in a lanthanum graphite intercalation compound," Phys. Rev. B **55**, 7927–7934 (1997).
[10] H. Yanagisawa, T. Tanaka, Y. Ishida, M. Matsue, E. Rokuta, S. Otani, and C. Oshima, "Analysis of phonons in graphene sheets by means of HREELS measurement and ab initio calculation," Surf. Interface Anal. **37**, 133–136 (2005).